NANO LETTERS
Cite This: Nano Lett. 2019, 19, 6299−6307
Letter
pubs.acs.org/NanoLett

Enhancing Photoluminescence and Mobilities in WS_2 Monolayers with Oleic Acid Ligands

Arelo O. A Tanoh,[†,‡] Jack Alexander-Webber,[§] James Xiao,[†] Géraud Delport,[†] Cyan A. Williams,[‡,∥] Hope Bretscher,[†] Nicolas Gauriot,[†] Jesse Allardice,[†] Raj Pandya,[†] Ye Fan,[§] Zhaojun Li,[†] Silvia Vignolini,[∥] Samuel D. Stranks,[†] Stephan Hofmann,[§] and Akshay Rao[†,*]

[†]Cavendish Laboratory, Cambridge, JJ Thomson Avenue, CB3 0HE, Cambridge, United Kingdom
[‡]Cambridge Graphene Centre, University of Cambridge, 9 JJ Thomson Avenue, Cambridge, CB3 0FA, Cambridge, United Kingdom
[§]Department of Engineering, University of Cambridge, JJ Thomson Avenue, CB3 0FA Cambridge, United Kingdom
[∥]Department of Chemistry, University of Cambridge, Lensfield Road, CB2 1EW, Cambridge, United Kingdom

S *Supporting Information*

ABSTRACT: Many potential applications of monolayer transition metal dichalcogenides (TMDs) require both high photoluminescence (PL) yield and high electrical mobilities. However, the PL yield of as prepared TMD monolayers is low and believed to be limited by defect sites and uncontrolled doping. This has led to a large effort to develop chemical passivation methods to improve PL and mobilities. The most successful of these treatments is based on the nonoxidizing organic "superacid" bis(trifluoromethane)sulfonimide (TFSI) which has been shown to yield bright monolayers of molybdenum disulfide (MoS_2) and tungsten disulfide (WS_2) but with trap-limited PL dynamics and no significant improvements in field effect mobilities. Here, using steady-state and time-resolved PL microscopy we demonstrate that treatment of WS_2 monolayers with oleic acid (OA) can greatly enhance the PL yield, resulting in bright neutral exciton emission comparable to TFSI treated monolayers. At high excitation densities, the OA treatment allows for bright trion emission, which has not been demonstrated with previous chemical treatments. We show that unlike the TFSI treatment, the OA yields PL dynamics that are largely trap free. In addition, field effect transistors show an increase in mobilities with the OA treatment. These results suggest that OA serves to passivate defect sites in the WS_2 monolayers in a manner akin to the passivation of colloidal quantum dots with OA ligands. Our results open up a new pathway to passivate and tune defects in monolayer TMDs using simple "wet" chemistry techniques, allowing for trap-free electronic properties and bright neutral exciton and trion emission.

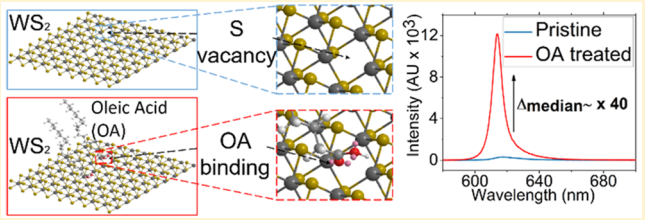

KEYWORDS: *Tungsten disulfide, ligand passivation, photoluminescence, mobilities*

Transition metal dichalcogenides (TMDs) are a class of layered materials which have garnered intense research interest due to their unique optical, electronic, and catalytic properties.[1−3] TMD bulk crystals consist of monolayers bound by weak van der Waals interactions, which can be overcome via dry mechanical cleavage (e.g., scotch tape method[4]) or via liquid phase exfoliation.[5,6] Also there are numerous ongoing efforts to directly grow highly crystalline few or monolayer TMD films in particular by chemical vapor deposition (CVD).[7,8] Many of these materials show a transition from indirect bandgap in the bulk material to a direct bandgap in the monolayer limit.[1,2] The direct band gap, high absorption coefficient, and potentially high carrier mobilities of TMD monolayers hold great potential for optoelectronic applications such as photodetectors, light emitting diodes (LEDs), and photovoltaics.[2] Reduced dielectric screening in TMD monolayers in contrast to the bulk crystal gives rise to tightly bound excitons at room temperature.[9,10] This provides an interesting arena to study many-body exciton−exciton and exciton−carrier interactions that result in diverse multiexciton[11,12] and charged exciton species[13,14] respectively.

A number of potential applications of TMDs, such as in optoelectronic devices, quantum light sources, or on-chip quantum information processing,[15−17] are dependent on having materials of high optical quality. In particular, there is a need for materials with high photoluminescence quantum efficiencies (PLQE) and also tunable emission properties. This raises a fundamental challenge for TMDs because exfoliated or CVD-prepared monolayers show extremely low PLQE, typically ∼0.001−5%.[18,19] There have been various proposals for the cause of the nonradiative exciton recombination such as trion formation,[20] the presence of chalcogen vacancies,[21] or other atomic substitutions.[22,23] However, the exact nature of the defects and the mechanism by which they quench PLQE is

Received: June 14, 2019
Revised: July 26, 2019
Published: August 16, 2019

DOI: 10.1021/acs.nanolett.9b02431
Nano Lett. 2019, 19, 6299−6307

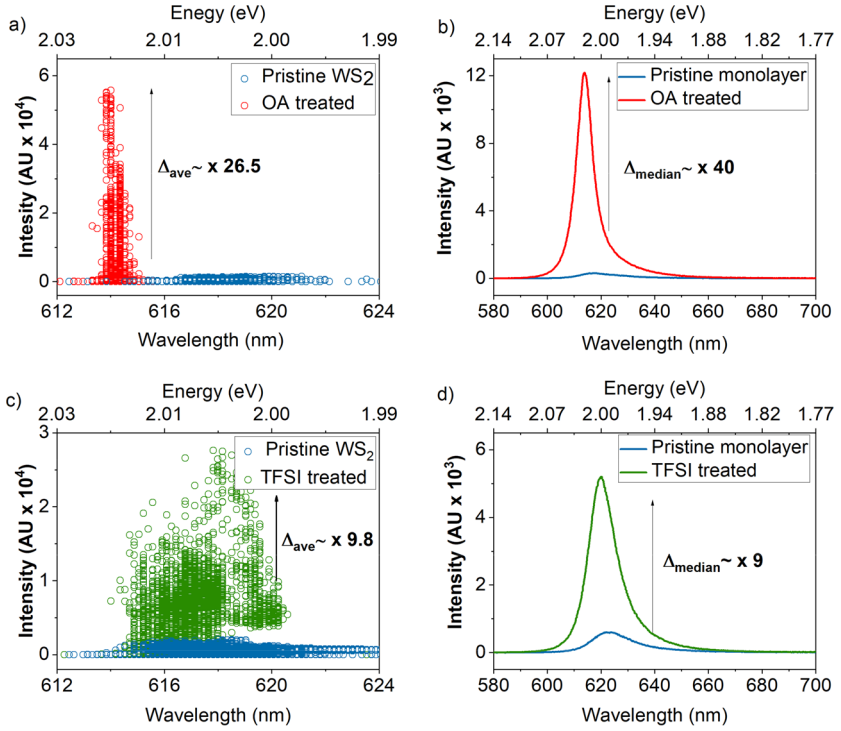

Figure 1. (a,c) PL enhancement scatter plot showing maximum untreated monolayer PL counts (blue) and peak OA (red) and TFSI (green) maximum treated monolayer PL counts measured at 135Wcm^{-2}. Data derived from nonfitted raw spectra from PL maps. (b,d) Raw PL spectra for points that represent the median peak PL counts before (blue) and after OA (red) and TFSI (green) treatment on exemplary monolayers.

still debated.[21,24−28] This has led to a number of treatments being proposed to enhance the PLQE of monolayer TMDs, most commonly MoS_2 and WS_2. For instance, studies have sought to improve PL via surface treatments using electron withdrawing dopants such as 2,3,5,6-tetrafluoro 7,7,8,8-tetracyanoquinodimethane (F4TCNQ)[20,29] and hydrogen peroxide.[30] Monolayer deposition of titanyl phthalocyanine (TiOPc) as a charge transfer interface also increases PL yield in MoS_2.[31] These are proposed to reduce electron density, suppressing low PLQE trion formation therefore promoting neutral exciton recombination. Other studies have sought to preserve the intrinsic optical properties of TMDs via exfoliation onto hexagonal boron nitride (hBN)[32] or hBN encapsulation,[33,34] which isolates monolayers from doping and disorder induced by the underlying substrate (e.g., Si−SiO_2). This has been shown to result in more uniformly distributed dominant neutral exciton PL with narrow homogeneous spectral line width free of substrate effects, which otherwise manifest as inhomogeneous contributions in monolayer TMD PL spectra.[33] Whereas hBN encapsulation improves overall optical quality, a large increase in PL at low excitation intensities has not been demonstrated. Hoshi et al.[35] have demonstrated that hBN encapsulation suppresses exciton−exciton annihilation rates in monolayer WS_2 as indicated by large PL enhancement at high excitation intensities compared with nonencapsulated monolayers. Most notably, surface treatment with nonoxidizing organic "super acid" bis-(trifluoromethane)sulfonimide (TFSI) has been shown to yield very bright PL from monolayer MoS_2 and WS_2. Although the exact mechanism of the PL enhancement is still debated, it has been shown that the TFSI treatment reduces the extent of n-type behavior in MoS_2,[21] which is consistent with the observed suppression of trion formation.[36] The authors of ref 21 have recently demonstrated PL enhancement and exciton dynamics similar to TFSI-treated MoS_2 and WS_2 via electric gating.[37] The application of a negative bias is said to dedope the intrinsically n-type materials, which suppresses trion formation thus enhancing radiative recombination of the neutral exciton. By comparing the exciton dynamics of TFSI-treated and gated TMDs, the authors conclude that TFSI acts as an electron drawing species which suppresses trion formation. However, it has been shown that the TFSI treatment leads to trap-limited PL dynamics[26] and does not give rise to improved mobilities in field-effect transistors.[21] In addition, the harsh nature of TFSI necessitates additional fabrication steps to protect commonly used electrode materials such as nickel.[21] Lastly, although treatments like the TFSI boost neutral exciton PL they do not lead to bright trion emission, which would be of use in applications such as optical readout of trions for spintronics.[38] Thus, an alternative benign chemical treatment that simultaneously improves PL and mobilities while easing device fabrication would provide an attractive means to functionalize and passivate monolayer TMDs.

Here, we demonstrate that a simple long-chain acid, oleic acid (OA) can greatly enhance the PL of monolayer WS_2 yielding bright neutral exciton emission comparable to TFSI treated monolayers. In addition, OA allows for bright trion emission and an increase in field effect mobilities. We also show that in comparison to previous TFSI treatment, where PL is trap limited, the OA treatment yields predominantly trap free PL characteristics. Our demonstration that a weak acid can be used to passivate and tune the properties of monolayers WS_2, draws parallels to the surface treatment of inorganic colloidal quantum dots, such as cadmium sulfide (CdS) and lead sulfide (PbS), where long-chain acids and in particular OA are used to passivate surfaces, and thus opens a range of

DOI: 10.1021/acs.nanolett.9b02431
Nano Lett. 2019, 19, 6299−6307

Table 1. PL Enhancement Statistics Derived from PL Maps of WS_2 Monolayers[a]

treatment	Δ_{ave}	σ_{counts}	λ_{ave}	σ_{λ}
OA	27	116%	618.3 nm*→614.2 nm	1.57 nm*→0.57 nm
TFSI	10	87.3%	618.4 nm*→617 nm	2.16 nm*→1.29 nm

[a]Characteristics prior to treatment marked with (*).

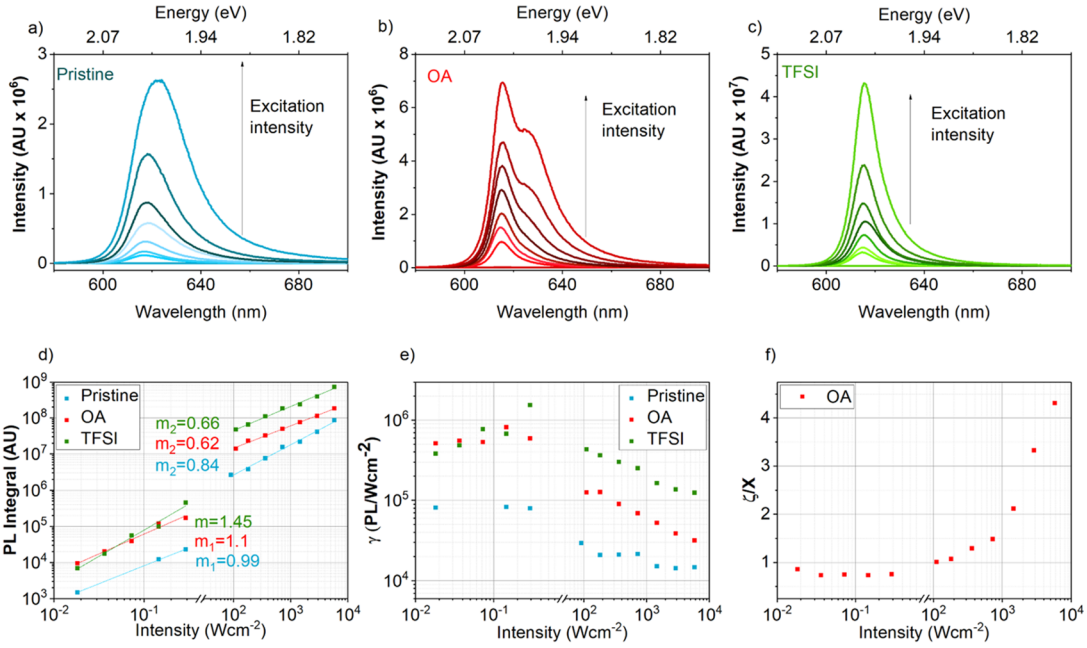

Figure 2. (a–c) Raw PL spectra of pristine, OA, and TFSI-treated samples taken with 514 nm CW laser. (d) Excitation series derived from PL integrals from panels a–c for pristine (blue), OA (red), and TFSI (green) treated monolayers. (e) Ratio of PL integral to excitation intensity, that is, relative PLQE (γ) variation with excitation intensity for pristine (blue), OA (red), and TFSI (green) treated monolayers. (f) Ratio of ζ and neutral exciton (X) peaks fitted from OA treated sample PL spectra to show increasing ζ to neutral exciton PL integral with increasing laser excitation intensity, indicating the presence of trions at high laser power

options for passivating and tuning the properties of monolayer TMDs.

Figure 1a,c shows the scatter plots of spectral position of the peak emission and peak PL counts extracted from PL maps of multiple WS_2 monolayers on Si-SiO_2 (90 nm) before and after surface treatment with OA and TFSI respectively. Maps were measured at 135 W cm^{-2}. Figure 1b,d shows representative PL spectra for points which correspond to the median PL intensity of an exemplary monolayer before and after treatment. Median enhancement factors, Δ_{median}, of 40× and 9× were calculated for OA and TFSI treatment, respectively. Table 1 shows key statistics that accompany PL enhancement, namely, average enhancement across the monolayers (Δ_{ave}), that is, the ratio of post- and pretreatment peak PL counts; standard deviation in PL intensity (σ_{counts}), average emission peak wavelength (λ_{ave}), and standard deviation in peak wavelength (σ_{λ}). The untreated case is indicated by (*) where appropriate. The data presented in Figure 1 and Table 1 were derived from nonfitted raw PL spectra.

For the data collected, the OA treated samples show a higher average enhancement factor compared to TFSI treated samples. The standard deviation in PL intensity, σ_{counts}, reveals that TFSI treatment results in a more spatially homogeneous brightness, as compared to the OA case. Better spectral uniformity is achieved with OA treatment as quantified by ~58% reduction in σ_{λ}, compared with a ~40% reduction in σ_{λ} with TFSI. The spectral narrowing in OA-treated monolayers is potentially due to changes in strain induced by ligand coordination. The statistical data derived from the PL maps clearly reveals that the OA treatment significantly improves the PL of the WS_2 monolayer.

In order to understand the exciton dynamics which underpin the PL enhancement with the OA treatment, we study the excitation intensity-dependent PL of the monolayers. Figure 2a–d shows the results derived from a room-temperature steady-state excitation intensity dependence series over 4 orders of magnitude to give insight into recombination regimes present in the samples. Because of experimental limitations, the excitation power was limited to low (0.018–0.3 W cm^{-2}) and high (110–5820 W cm^{-2}) regimes, making sure to remain below 9000 W cm^{-2} to avoid thermal damage.[39,24]

Figure 2a shows noticeable changes in spectral shape with increasing excitation intensity in the pristine monolayer. The spectra appear to broaden and red shift. This spectral red shift with increasing excitation intensity in pristine monolayers has been attributed to trion (X^-) formation, which occurs as a result of binding between excess charges in the conduction band from photoionized native n-dopants and neutral excitons (X).[40] With large binding energies of the order of tens of millielectronvolts due to reduced screening in monolayers, these quasi-particles can be observed and studied at ambient conditions.[13]The perceived red shift and spectral broadening as a function of excitation intensity is caused by the contributions of trions alongside excitons. The close overlap between the excitons and trions makes deconvoluting the spectra challenging, which prevents resolution of the relative

DOI: 10.1021/acs.nanolett.9b02431
Nano Lett. 2019, 19, 6299–6307

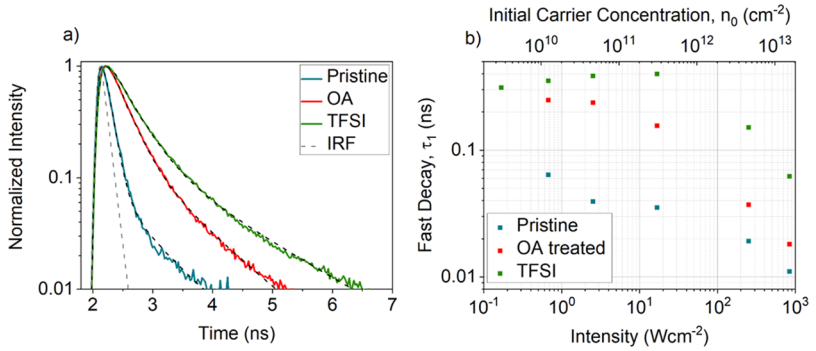

Figure 3. (a) Time-resolved PL signals of pristine (blue), OA (red), and TFSI (green) treated WS_2 monolayers with biexponential decay fits (black dashed lines), measured at 0.67 Wcm^{-2} pump intensity with 405 nm excitation. (b) Variation of fast decay component, τ_1, with initial carrier concentration derived from absorption data (SI Figure 3) at pump wavelength (405 nm) and pump intensities (Wcm^{-2}).

contributions from excitons and trions. We also note the narrower spectral line width in OA treated WS_2 on Si-SiO_2 shown in Figure 1b compared with that on quartz (Figure 2b) at similar excitation intensities. The difference in spectral line width is potentially due to variations in strain and/or dielectric environment between the substrates. These factors may also contribute to spectral broadening,[32] which in this case appears to be more present on quartz. For clarity, the normalized spectra are shown in SI Figure 6.

Figure 2b shows comparable data for the OA treated monolayer. In the high excitation intensity regime (10^2–10^4 W cm^{-2}) in addition to the neutral exciton peak (which does not shift in energy), a red-shifting peak, ζ, emerges. The well separated ζ-feature enables spectral fitting with Gaussians as shown in Supporting Information (SI) Figure 1. Figure 3f shows the increasing ratio of ζ-peak intensity to the neutral exciton (X) as a function of excitation intensity, which is a notable characteristic of trion (X^-) emission.[41] SI Section 1 provides further description and brief analysis of results acquired from spectral fits. Figure 3c shows the spectra for the TFSI-treated sample, where the single narrow emission peak throughout the series indicates dominant neutral exciton recombination, which is consistent with what has been reported in ref 21.

Figure 2d shows a log–log plot of the PL intensity dependence as a function of excitation intensity for each sample. Under low power excitation, the brightness of the OA treated sample is comparable to the TFSI treated sample. The gradients of the series in the two regions give insight into the recombination regimes present. The gradient values are the exponent to a power law fit given by $I = P^m$.[24] Figure 2e shows the ratio of PL to excitation intensity (γ), which serves as a relative PLQE value. At low intensities, the pristine sample shows near-linear behavior (m_1 = 0.99) with respect to excitation intensity, as expected of band-edge to ground-state recombination and little variation in its low γ ratios reflective of inherently low PLQE. At high intensities,the trend become sublinear (m_2 0.84). This suggests the presence of nonradiative exciton–exciton annihilation, however, given its low effective PLQE (i.e., low γ), nonradiative defect-assisted processes dominate exciton dynamics in both regimes.

When treated with OA, an enhancement in PL under low intensity comparable to the TFSI case is evident but with a power law exponent close to the pristine case (m_1 = 1.1). The γ-ratio increases only slightly, indicating predominant radiative neutral exciton directly from the band edge in the low intensity regime. At high laser intensities, the power law diminishes more drastically than the pristine case (m_2 = 0.62). As previously discussed for Figure 2b,f at higher excitation intensity there is a large contribution of trions to its overall emission. Given the inherently lower PLQE of trions compared to neutral excitons, the reduction in overall radiative recombination rate due in part to trion generation in the high power regime is plausible. In effect, a combination of exciton–exciton annihilation, trion generation, and any persisting defect related nonradiative decay mechanisms should account for the overall reduction in γ seen in the OA treated sample.

Interestingly, the TFSI treated sample shows superlinear (m_1 = 1.45) behavior and increasing γ-ratio (i.e., relative PLQE) at low intensity. This manifests itself as a dependence of the relative PLQE on excitation intensity, as seen in Figure 2e. The study by Goodman et al.[26] on long-lived trapped excitons in defect states best explains this observed superlinear behavior. At the low end of the low intensity regime, a proportion of excitons decay from traps to the ground state over a long period (~μs). These long-lived low energy transitions form part of the tail-end region of the PL spectra.[42] Available ambient thermal energy at room temperature statistically favors detrapping for a significant proportion of trapped excitons, which return to the band edge and recombine radiatively to the ground state. With increasing excitation, density traps become saturated causing any further excitations to recombine radiatively directly from the band edge. Hence, the superlinear behavior and increasing γ-ratio in the low intensity regime characterizes the process of trap state filling prior to predominant radiative recombination where the effective PLQE (γ) saturates. The diminishing γ-ratio in the high-intensity regime signifies the onset of exciton–exciton annihilation.[21,24]

To explore the photophysics of the treatment further we turn to time-resolved PL microscopy. Figure 3a shows normalized time-resolved signal of untreated and treated samples at room temperature under low power excitation (0.67 W cm^{-2}). Biexponential decay fits best describe the decay dynamics observed with a fast component τ_1 and a slow component τ_2. The fast decay (τ_1 ~ 64 ps) of the pristine sample indicates a pronounced onset nonradiative recombination at early times, consistent with the intrinsically low PLQE. The OA and TFSI-treated samples show a signal growth beyond the instrument response function (IRF) region. Although the exact nature of this growth in the PL signal is

DOI: 10.1021/acs.nanolett.9b02431
Nano Lett. 2019, 19, 6299–6307

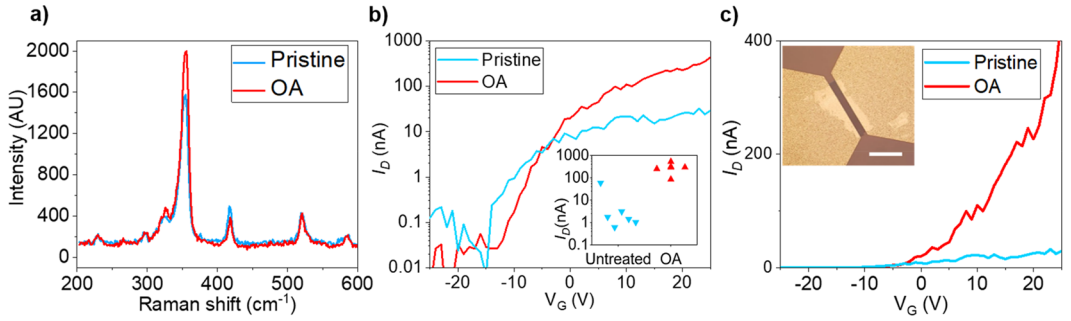

Figure 4. (a) Raman spectra of a WS_2 transistor before and after OA treatment. (b,c) Transfer characteristics of a WS_2 transistor measured on the same flake before and after OA treatment at V_{DS} = 10 V. The arrows indicate the gate voltage sweep direction. (Inset b) On state current I_D at back gate voltage V_G = 25 V for six devices before (red) and after (blue) OA treatment. (Inset c) Image of transistor structure with scale bar measuring 20 μm.

unclear, it might be related with trapping and detrapping dynamics at early times. The OA treatment gives rise to a 4× increase in lifetime for the fast decay component ($\tau_1 \sim 248$ ps) versus the pristine sample, close to the TFSI-treated sample ($\tau_1 \sim 310$ ps), which is expected by nature of the improved PLQE for these samples and suggests a suppression of the early time quenching observed in the pristine sample.

Figure 3b shows the variation in the fast decay component (τ_1) as a function of initial carrier concentration (n_0). As shown in SI Figure 4a–c, at the maximum intensity (842 W cm^{-2}) the OA and pristine decay signal fit a single exponential decay, whereas the TFSI signals follow the biexponential model throughout the series. The extremely fast initial decay times (tens of picoseconds) in the pristine samples even at the low end of the initial carrier concentration range implies the presence of a strong quenching channel. Further reduction in τ_1 as a function of n_0 confirms the presence of exciton–exciton annihilation.

The continuous reduction in τ_1 as a function of n_0 in the OA-treated sample implies nontrap limited movement of excitons that are able to annihilate even at low carrier concentrations. At higher excitation intensities the formation of low PLQE trions, as seen in Figure 2b, will contribute to the sharp reduction in τ_1. The TFSI treated sample's gradual increase in τ_1 at lower initial carrier concentrations is in agreement with the increase in relative PLQE (γ) in the low intensity (steady-state) excitation regime shown in Figure 2e. At low excitation densities, a proportion of trap states are filled, and any further transition from the band edge to those states is forbidden, which promotes direct recombination from the band edge with τ_1. As carrier concentration increases, trap states are filled giving rise to dominant radiative recombination from the band edge as indicated by the saturated τ_1 value. The reduction in τ_1 at high carrier concentrations signals the onset of exciton–exciton annihilation.[24] The slow component, τ_2, as a function of n_0 is shown in SI Figure 4d shows similar behavior.

To summarize the photophysical measurements presented so far, the OA treatment is found to greatly increase the PL of monolayer WS_2, with average increases higher than TSFI treatment. At higher excitation intensities, a pronounced trion peak emerges which is not found in TFSI-treated samples. Both steady-state and time-resolved measurements indicate that the OA treatment leads to trap-free excitonic behavior in contrast to TFSI treatment where trap-limited behavior is observed, consistent with previous reports. This suggests that the mechanism of PL enhancement for the OA and TFSI are quite different.

Various studies identify chalcogen point defects, which manifest themselves as subgap states through which nonradiative emission occurs as the prime cause of poor quantum yields in pristine TMD monolayers.[43,44] Chalcogen point defect passivation via surface treatment is often used as the basis to explain the observed PL improvements with TFSI treatment. Although the exact mechanism of such treatment is unclear,[21,28,27] it has been suggested that TFSI being a super acid ($pK_a = -12.3$) protonates the native n-doped monolayer surface, removing excess dopants or charges occupying existing trap/defect states.[21] The freeing up of defect sites gives rise to the trap limited exciton dynamics, as has been discussed by Goodman et al.[26] Atallah et al.[45] however propose that electrons in the n-type TMD material reduce protons (H^+) to hydrogen (H_2), leaving the TFSI counterion ($[(CF_3SO_2)_2N]^-$) to passivate the positively charged defect sites. The observation of excitons decaying to the trap states by Goodman et al.[26] is, however, at odds with the notion of passivation of point defects by the TFSI counterion, as true passivation would block the movement of excitons to trap states and thus promote direct band-edge recombination. In contrast, as we have shown in Figure 2 and 3, the OA treatment leads to nontrap limited exciton dynamics, while also giving high PL yield. This suggests that the OA is passivating defect sites.

OA is a weak acid and, unlike TFSI, cannot effectively protonate the monolayer TMD surface and reduce n-doping (this is confirmed by the transistor measurements described below). The electron-rich carboxylic acid moiety is a good coordinating group and OA is commonly used as ligands in stabilizing colloidal quantum dots, providing steric and electronic passivation of surface defects, for example, dangling bonds caused by sulfur vacancies on lead sulfide (PbS) quantum dots.[46–48] It is therefore reasonable to speculate that the observed improvements in emission could be due to similar passivation, where the carboxylate group behaves as a Lewis base, coordinating to the electrophilic metal (W) atom at the S vacancy forming a dative covalent bond. The W atoms in WS_2 possess an unfilled d-orbital due to the energetic gap between the 6s and 5d orbitals. The empty d-orbital does not contribute to covalent bonding and the band structure within monolayer WS_2. The empty orbital provides a binding site for OA as a ligand. At vacancy sites, the ligand attachment increases localized electron density and provides mitigation for the nonradiative loss channels at defect sites which are normally

DOI: 10.1021/acs.nanolett.9b02431
Nano Lett. 2019, 19, 6299–6307

electron-deficient. This increased electron density at these sites may contribute toward the observed additional trion formation at higher excitation intensities. In addition, binding of oleic acid to the monolayer surface provides a hydrophobic long alkyl chain providing a steric and dielectric barrier toward other mechanisms of nonradiative loss mechanisms such as interactions with adsorbates including oxygen and water.

Lastly, we explore what impact the OA treatment has on charge transport in WS_2. Figure 4b,c shows the transfer characteristics of the same monolayer WS_2 field effect transistor (FET) before and after OA treatment. Raman spectroscopy of the treated transistors confirm there are no discernible structural changes (Figure 4a). After OA treatment the on-state current, measured at back gate voltage V_G = 25 V, consistently improves for all of the devices studied (six devices in total) from an average of 11 nA before to 290 nA after (Figure 4b, inset). The device maintains n-type behavior. This confirms that the OA does not significantly dope the monolayer, as is the case for TFSI.[37] The field effect mobility improves from 5×10^{-4} $cm^2/(V\ s)$ to 1×10^{-2} $cm^2/(V\ s)$, a factor of 20, after OA treatment. The absolute values of field effect mobility are likely limited by contact resistance and could be further improved using recent developments in contact engineering such as van der Waals contacts.[49] The subthreshold swing decreases from 16 to 8 V/dec (Figure 4b), indicating a reduction in the interface charge trap density in the presence of ligands, which supports the notion of ligand passivating traps. The increase in drain current may also be due to an injection of charges from the electron rich coordinating ligand carboxylate group to the conduction band of the electron deficient metal species at a vacancy. The transfer characteristics confirm that at V_G = 0 V, there are mobile electrons available in the conduction band to form trions with excitons under high intensity photoexcitation as described above. We note that we did not need to protect the contact regions during oleic acid treatment and all of the devices studied showed similar behavior (Figure 4b). By contrast, TFSI is known to etch several common contact metals and protective layers were required to prevent deterioration of the contact region during treatment in previous studies.[21] When using TFSI without a protective layer we obtain a very low yield of working devices. For the single measurable device, we observe a shift from n-type to p-type field effect behavior as shown in SI Figure 7, with an initial FET electron mobility of 5×10^{-3} $cm^2/(V\ s)$ switching to 2×10^{-3} $cm^2/(V\ s)$ FET hole mobility once treated. This change in transport behavior is consistent with Lien et al's observation of hole-doping by TFSI on TMD FETs with palladium (Pd) contacts.[37] Importantly, however, our results show that it is possible to dramatically improve the PL of monolayer WS_2 while improving mobility and reducing charge trapping without additional device fabrication steps using OA.

In conclusion, we have demonstrated the ability to significantly increase the PL in monolayer WS_2 via surface treatment with OA ligands. Statistical analysis shows that the OA improved spectral uniformity as compared to untreated and TFSI treated samples. Steady-state excitation intensity and time-resolved pump-intensity studies reveal trap free exciton dynamics unlike the trap-limited dynamics observed in TFSI-treated samples,[26] which is taken as an indication of defect passivation by the ligands. In support of this hypothesis, electrical transport characteristics of OA treated WS_2 transistors show an increase in field effect mobilities, reduced charge trap density, and no detectable additional doping upon treatment with OA. At increased excitation densities, we observe bright trion emission, which is not observed with the TFSI treatment. These bright trions may be of interest for future spintronics and quantum information applications. Although future experimental and theoretical work is required to elucidate the exact chemical changes that accompany the OA treatment, we hypothesize that the carboxylate group forms a dative covalent bond with the electrophilic metal atom (W) at a chalcogen vacancy, similar to the passivation of PbS quantum dots with OA. This trap state passivation by the ligand forbids nonradiative trap-assisted exciton decay, promoting direct radiative band edge recombination. Our results open up a new pathway to passivate and tune defects in monolayer TMDs using simple wet chemistry techniques, allowing for trap free electronic properties and bright neutral exciton and trion emission.

Experimental Methods. *Material Preparation and Initial Characterization.* Prior to exfoliation, substrates were solvent processed via sonication in acetone and isopropyl alcohol (IPA) for ∼15 min and treated in O_2 plasma to remove adsorbants. Silicon−silicon dioxide (Si−SiO_2) substrates with 90 nm oxide layer were used for steady-state PL, Raman spectroscopy, and electronic characterization, whereas quartz substrates were used for steady-state excitation intensity series time-resolved PL measurements.

Large area WS_2 monolayers were prepared via gold-mediated exfoliation.[50] The bulk crystal purchased from 2D semiconductors was exfoliated manually onto clean-room tape prior to depositing a thin gold layer (∼100−150 nm) via thermal evaporation in a thermal evaporator under vacuum conditions. Following gold evaporation, thermal release tape was adhered to the gold-coated WS_2 exfoliate, whereupon the cleanroom tape was peeled off, leaving the topmost layer of WS_2 attached to the gold on thermal tape. The thermal tape was then stuck onto the freshly plasma-treated target substrate and heated on a hot plate up to 125 °C, whereupon the thermal tape peals leaving the TMD monolayers sandwiched between the gold and substrate. The excess gold was removed by immersing in potassium iodide (KI_2) and iodine (I_2) standard gold etch (Sigma-Aldrich). The substrate was gently swirled in the etchant for 4 min prior to rinsing in deionized water, 10 min sonication in acetone, and 5 min rinse in isopropyl alcohol (IPA). Samples were dried with a nitrogen (N_2) gun. Monolayers were initially identified via the optical contrast method.[51]

OA Treatment. In a nitrogen glovebox, the exfoliated monolayer TMD samples were submerged in degassed OA (Sigma-Aldrich) contained in 60 mL vials. The vials were placed on a hot plate set to 25 °C for 12 h overnight after which the samples were rinsed in anhydrous toluene and blow dried with a N_2 gun. The OA may also be drop casted. PL spectroscopy reveals that the toluene rinse slightly improves PL as shown in SI Figure 5. This is considered a result of surface cleaning which may remove some adsorbants that quench PL.

TFSI Preparation and Treatment. Following Amani et al.,[21] 2 mg/mL of acid was prepared in a nitrogen glovebox by dissolving 20 mg of TFSI crystals in 10 mL of 1,2-dicholoroethane (DCE). Further dilution produced a 0.2 mg/mL solution of acid. The TMD sample was immersed in the acid and tightly closed vial for 40 min at room

DOI: 10.1021/acs.nanolett.9b02431
Nano Lett. 2019, 19, 6299−6307

temperature.[25] After treatment, the sample was removed and dried with a N_2 gun.

Steady-State Absorption Spectroscopy. The absorption spectra of monolayer WS_2 on quartz were measured with a Zeiss axiovert inverted microscope in transmission using a halogen white light source via a Zeiss EC Epiplan Apochromat 50× objective (numerical aperture (NA) = 0.95) forming a collection area diameter measured at 10 μm with the field of view and aperture fully opened. Light transmitted via the sample was split via beam splitter with one component directed to a CCD camera (DCC3240C, Thorlabs) and the other coupled to a UV600 nm optical fiber (200−800 nm spectral range) connected to a spectrometer (Avaspec-HS2048, Avantes).

Steady-State PL Spectroscopy. All samples were characterized via steady state PL to confirm monolayer identity before and after treatment. PL spectroscopy was performed on a Renishaw Invia confocal setup equipped with motorized piezo stage, using an air-cooled Ar-ion 514.5 nm continuous wave (CW) laser via 50× objective (NA = 0.75). Signals were collected in reflection via notch filter. The diffraction limited beam spot size was estimated as 0.84 μm. PL signal was dispersed via a 600 L/mm grating prior to detection with inbuilt CCD detector. Laser power was measured directly via 5× objective with a Thorlabs S130C photodiode and PM100D power meter.

PL maps were generated from multiple WS_2 monolayers before and after respective chemical treatments. For the OA treated sample, five monolayers on a single substrate were mapped prior to treatment. Following treatment, two out of five were delaminated, most likely due to surface tension effects exerted by OA. The remaining three treated monolayers were measured in PL and compared to their untreated cases. For TFSI, five untreated monolayers on a single substrate were mapped and remained intact following treatment. Maps were generated with 0.5 μm resolution and 0.5 s integration time at 0.75 μW with cosmic ray correction engaged via the microscope's WIRE software.

Steady-state PL intensity series were performed on the WS_2 monolayers deposited on quartz. Care was taken to measure PL in the same locations prior to and following treatment. The spatial x, y, and z focal plane of the measurement site and photodiode were recorded to accurately switch between photodiode and monolayer location for each PL measurement using the WIRE software piezo stage control interface. PL signals were scaled up to 500 s integration time used on the lowest excitation intensity. Dark counts were measured for each measurement in the series with the same integration time and subtracted from raw PL data.

Trion and neutral exciton emission were deconvoluted from OA treated WS_2 PL signals with dark counts subtracted using a procedure written in Matlab, which incorporates the "gauss2" two Gaussian model fit. Further information on the Gaussian model is available via the mathsworks Web site.

Time-Resolved PL Microscopy. Time-resolved PL measurements were performed on the same samples on quartz prior to and following treatment. A PicoQuant Microtime 200 confocal time-resolved PL setup equipped using 405 nm pulsed laser excitation via 20× objective (NA = 0.4) with estimated diffraction limited spot size of ∼1.23 μm. The repetition rate was set to 20 MHz with 25 ps resolution used to obtain time-resolved PL data. All signals were integrated for 300 s and collected in transmission. Signals were detected with a photomultiplier tube (PMT). Instrument response functions were measured with blank quartz substrates at each power used in the intensity series. Power was measured using an inbuilt photodetector at each intensity and read via the microscope's software interface. Care was taken to ensure that excitation was performed in the same spot on the monolayers prior to and following treatment. PL decay data were fitted with the aid of an openly available Matlab based deconvolution procedure, fluofit devised by Jorg Enderlein.[52] The URL for this code is provided in SI.

Transistor Preparation and Characterization. As-exfoliated isolated WS_2 flakes on doped Si (used as global back gate) covered with 90 nm of thermally grown SiO_2 were identified through optical microscopy and PL spectroscopy. Electrical contacts were defined by electron beam lithography followed by thermal evaporation of indium/gold (In/Au) (10 nm/80 nm). Transfer characteristics were measured with a source drain bias of V_{DS} = 10 V using a Keithley 4200-SCS parameter analyzer and probe station under dark ambient conditions.

FET Raman Characterization. Field effect transistors (FETs) were characterized via Raman spectroscopy with the Renishaw Invia confocal setup described, at 0.7 μW with 50× objective. The Raman signal was collected in reflection via notch filter and dispersed via 2400 L/mm grating prior to detection.

TOC Design. TOC nanocrystal graphics were developed in VESTA software[53] and parsed into ChemDraw3D (PerkinElmer) for rendering.

■ ASSOCIATED CONTENT

Supporting Information

The Supporting Information is available free of charge on the ACS Publications website at DOI: 10.1021/acs.nanolett.9b02431.

Additional information includes detailed analysis of trion emission characterization, time-resolved PL decay fitting code URL, spectral deconvolution of OA treated WS_2 PL spectra using Gaussian fits, various trion and neutral exciton characteristics derived from preceding Gaussian fits of OA treated WS_2 PL spectra, WS_2 steady state absorption spectrum, time-resolved PL spectra for all treatments and variation of slow decay component with initial carrier concentration, effect of toluene on WS_2 PL, PL spectral line width comparison between OA treated WS_2 on Si−SiO_2 and quartz respectively, and transfer characteristics of WS_2 transistor treated with TFSI (PDF)

■ AUTHOR INFORMATION

ORCID

Arelo O. A Tanoh: 0000-0003-2494-5984
Jack Alexander-Webber: 0000-0002-9374-7423
Raj Pandya: 0000-0003-1108-9322
Silvia Vignolini: 0000-0003-0664-1418
Samuel D. Stranks: 0000-0002-8303-7292
Stephan Hofmann: 0000-0001-6375-1459
Akshay Rao: 0000-0003-4261-0766

Author Contributions

A.O.A.T. thanks H.B. and N.G. for assistance in sample preparation, G.D. for time-resolved PL measurements, J.A. for discussions on time-resolved PL data, J.A.-W. and Y.F. for

DOI: 10.1021/acs.nanolett.9b02431
Nano Lett. 2019, 19, 6299−6307

transistor preparation, electrical characterization, and data interpretation, C.A.W. for steady state absorption measurements;, J.X. for discussions on surface chemistry, and Z.L for assistance in preparing TOC graphics.

Notes

The authors declare no competing financial interest.

■ ACKNOWLEDGMENTS

The authors thank the Winton program for physics of sustainability for financial support. We also acknowledge funding from EPSRC Grants EP/L015978/1, EP/L016087/1, EP/P027741/1, EP/M006360/1, and EP/P005152/1. J.A.-W. acknowledges the support of his Research Fellowship from the Royal Commission for the Exhibition of 1851. G.D. would like to acknowledge the Royal Society for funding the Newton International fellowship. S.D.S acknowledges support from the Royal Society and Tata Group (UF150033). This project has received funding from the European Research Council (ERC) under the European Union's Horizon 2020 research and innovation programme (Grant Agreements 758826 and 756962). The data underlying this publication are available at DOI 10.17863/CAM.42980.

■ REFERENCES

(1) Mak, K. F.; Lee, C.; Hone, J.; Shan, J.; Heinz, T. F. Atomically Thin MoS_2: A New Direct-Gap Semiconductor. *Phys. Rev. Lett.* **2010**, *105*, 136805.

(2) Mak, K. F.; Shan, J. Photonics and Optoelectronics of 2D Semiconductor Transition Metal Dichalcogenides. *Nat. Photonics* **2016**, *10* (4), 216−226.

(3) Liu, H. L.; Shen, C. C.; Su, S. H.; Hsu, C. L.; Li, M. Y.; Li, L. J. Optical Properties of Monolayer Transition Metal Dichalcogenides Probed by Spectroscopic Ellipsometry. *Appl. Phys. Lett.* **2014**, *105* (20), 201905.

(4) Geim, A. K.; Novoselov, K. S. The Rise of Graphene. *Nat. Mater.* **2007**, *6* (3), 183−191.

(5) Shen, J.; He, Y.; Wu, J.; Gao, C.; Keyshar, K.; Zhang, X.; Yang, Y.; Ye, M.; Vajtai, R.; Lou, J.; et al. Liquid Phase Exfoliation of Two-Dimensional Materials by Directly Probing and Matching Surface Tension Components. *Nano Lett.* **2015**, *15* (8), 5449−5454.

(6) Nicolosi, V.; Chhowalla, M.; Kanatzidis, M. G.; Strano, M. S.; Coleman, J. N. Liquid Exfoliation of Layered Materials. *Science* **2013**, *340* (6139), 1226419.

(7) Kang, K.; Xie, S.; Huang, L.; Han, Y.; Huang, P. Y.; Mak, K. F.; Kim, C. J.; Muller, D.; Park, J. High-Mobility Three-Atom-Thick Semiconducting Films with Wafer-Scale Homogeneity. *Nature* **2015**, *520* (7549), 656−660.

(8) Briggs, N.; Subramanian, S.; Lin, Z.; Li, X.; Zhang, X.; Zhang, K.; Xiao, K.; Geohegan, D.; Wallace, R.; Chen, L. Q. A Roadmap for Electronic Grade 2D Materials. *2D Mater.* **2019**, *6* (2), 022001.

(9) Berkelbach, T. C.; Hybertsen, M. S.; Reichman, D. R. Theory of Neutral and Charged Excitons in Monolayer Transition Metal Dichalcogenides. *Phys. Rev. B: Condens. Matter Mater. Phys.* **2013**, *88* (4), 045318.

(10) Ye, Z.; Cao, T.; O'Brien, K.; Zhu, H.; Yin, X.; Wang, Y.; Louie, S. G.; Zhang, X. Probing Excitonic Dark States in Single-Layer Tungsten Disulphide. *Nature* **2014**, *513* (7517), 214−218.

(11) You, Y.; Zhang, X. X.; Berkelbach, T. C.; Hybertsen, M. S.; Reichman, D. R.; Heinz, T. F. Observation of Biexcitons in Monolayer WSe 2. *Nat. Phys.* **2015**, *11* (6), 477−481.

(12) Qiu, D. Y.; Da Jornada, F. H.; Louie, S. G. Optical Spectrum of MoS_2: Many-Body Effects and Diversity of Exciton States. *Phys. Rev. Lett.* **2013**, *111* (21), 216805.

(13) Mak, K. F.; He, K.; Lee, C.; Lee, G. H.; Hone, J.; Heinz, T. F.; Shan, J. Tightly Bound Trions in Monolayer MoS 2. *Nat. Mater.* **2013**, *12* (3), 207−211.

(14) Barbone, M.; Montblanch, A. R. P.; Kara, D. M.; Palacios-Berraquero, C.; Cadore, A. R.; De Fazio, D.; Pingault, B.; Mostaani, E.; Li, H.; Chen, B.; et al. Charge-Tuneable Biexciton Complexes in Monolayer WSe_2. *Nat. Commun.* **2018**, *9* (1), 3721.

(15) Lagoudakis, K. G.; McMahon, P. L.; Dory, C.; Fischer, K. A.; Müller, K.; Borish, V.; Dalacu, D.; Poole, P. J.; Reimer, M. E.; Zwiller, V.; et al. Ultrafast Coherent Manipulation of Trions in Site-Controlled Nanowire Quantum Dots. *Optica* **2016**, *3* (12), 1430.

(16) Ross, J. S.; Wu, S.; Yu, H.; Ghimire, N. J.; Jones, A. M.; Aivazian, G.; Yan, J.; Mandrus, D. G.; Xiao, D.; Yao, W.; et al. Electrical Control of Neutral and Charged Excitons in a Monolayer Semiconductor. *Nat. Commun.* **2013**, DOI: 10.1038/ncomms2498.

(17) Wang, K.; De Greve, K.; Jauregui, L. A.; Sushko, A.; High, A.; Zhou, Y.; Scuri, G.; Taniguchi, T.; Watanabe, K.; Lukin, M. D.; et al. Electrical Control of Charged Carriers and Excitons in Atomically Thin Materials. *Nat. Nanotechnol.* **2018**, *13* (2), 128−132.

(18) Wang, H.; Zhang, C.; Rana, F. Ultrafast Dynamics of Defect-Assisted Electron-Hole Recombination in Monolayer MoS_2. *Nano Lett.* **2015**, *15* (1), 339−345.

(19) Ross, J. S.; Klement, P.; Jones, A. M.; Ghimire, N. J.; Yan, J.; Mandrus, D. G.; Taniguchi, T.; Watanabe, K.; Kitamura, K.; Yao, W.; et al. Electrically Tunable Excitonic Light-Emitting Diodes Based on Monolayer WSe_2 p-n Junctions. *Nat. Nanotechnol.* **2014**, *9* (4), 268−272.

(20) Mouri, S.; Miyauchi, Y.; Matsuda, K. Tunable Photoluminescence of Monolayer MoS_2 via Chemical Doping. *Nano Lett.* **2013**, *13* (12), 5944−5948.

(21) Amani, M.; Lien, D. H.; Kiriya, D.; Xiao, J.; Azcatl, A.; Noh, J.; Madhvapathy, S. R.; Addou, R.; Santosh, K. C.; Dubey, M.; et al. Near-Unity Photoluminescence Quantum Yield in MoS2. *Science* **2015**, *350* (6264), 1065−1068.

(22) Barja, S.; Refaely-Abramson, S.; Schuler, B.; Qiu, D. Y.; Pulkin, A.; Wickenburg, S.; Ryu, H.; Ugeda, M. M.; Kastl, C.; Chen, C.; et al. Identifying Substitutional Oxygen as a Prolific Point Defect in Monolayer Transition Metal Dichalcogenides with Experiment and Theory. **2018**, *arxiv:1810.03364* (accessed on May 19, 2019).

(23) Pető, J.; Ollár, T.; Vancsó, P.; Popov, Z. I.; Magda, G. Z.; Dobrik, G.; Hwang, C.; Sorokin, P. B.; Tapasztó, L. Spontaneous Doping of the Basal Plane of MoS 2 Single Layers through Oxygen Substitution under Ambient Conditions. *Nat. Chem.* **2018**, *10* (12), 1246−1251.

(24) Amani, M.; Taheri, P.; Addou, R.; Ahn, G. H.; Kiriya, D.; Lien, D. H.; Ager, J. W.; Wallace, R. M.; Javey, A. Recombination Kinetics and Effects of Superacid Treatment in Sulfur- and Selenium-Based Transition Metal Dichalcogenides. *Nano Lett.* **2016**, *16* (4), 2786−2791.

(25) Kim, H.; Lien, D. H.; Amani, M.; Ager, J. W.; Javey, A. Highly Stable Near-Unity Photoluminescence Yield in Monolayer MoS2 by Fluoropolymer Encapsulation and Superacid Treatment. *ACS Nano* **2017**, *11* (5), 5179−5185.

(26) Goodman, A. J.; Willard, A. P.; Tisdale, W. A. Exciton Trapping Is Responsible for the Long Apparent Lifetime in Acid-Treated MoS_2. *Phys. Rev. B* **2017**, *96* (12), No. 121404.

(27) Roy, S.; Choi, W.; Jeon, S.; Kim, D. H.; Kim, H.; Yun, S. J.; Lee, Y.; Lee, J.; Kim, Y. M.; Kim, J. Atomic Observation of Filling Vacancies in Monolayer Transition Metal Sulfides by Chemically Sourced Sulfur Atoms. *Nano Lett.* **2018**, *18* (7), 4523−4530.

(28) Lu, H.; Kummel, A.; Robertson, J. Passivating the Sulfur Vacancy in Monolayer MoS_2. *APL Mater.* **2018**, *6* (6), 066104.

(29) Peimyoo, N.; Yang, W.; Shang, J.; Shen, X.; Wang, Y.; Yu, T. Chemically Driven Tunable Light Emission of Charged and Neutral Excitons in Monolayer WS 2. *ACS Nano* **2014**, *8* (11), 11320−11329.

(30) Su, W.; Dou, H.; Li, J.; Huo, D.; Dai, N.; Yang, L. Tuning Photoluminescence of Single-Layer MoS_2 Using H_2O_2. *RSC Adv.* **2015**, *5* (101), 82924−82929.

(31) Park, J. H.; Sanne, A.; Guo, Y.; Amani, M.; Zhang, K.; Movva, H. C. P.; Robinson, J. A.; Javey, A.; Robertson, J.; Banerjee, S. K.; et al. Defect Passivation of Transition Metal Dichalcogenides via a

DOI: 10.1021/acs.nanolett.9b02431
Nano Lett. 2019, 19, 6299−6307

Charge Transfer van Der Waals Interface. *Sci. Adv.* **2017**, *3* (10), No. e1701661.
(32) Courtade, E.; Han, B.; Nakhaie, S.; Robert, C.; Marie, X.; Renucci, P.; Taniguchi, T.; Watanabe, K.; Geelhaar, L.; Lopes, J. M. J.; et al. Spectrally Narrow Exciton Luminescence from Monolayer MoS_2 and $MoSe_2$ Exfoliated onto Epitaxially Grown Hexagonal BN. *Appl. Phys. Lett.* **2018**, *113* (3), 032106.
(33) Ajayi, O. A.; Ardelean, J. V.; Shepard, G. D.; Wang, J.; Antony, A.; Taniguchi, T.; Watanabe, K.; Heinz, T. F.; Strauf, S.; Zhu, X. Y. Approaching the Intrinsic Photoluminescence Linewidth in Transition Metal Dichalcogenide Monolayers. *2D Mater.* **2017**, *4* (3), 031011.
(34) Cadiz, F.; Courtade, E.; Robert, C.; Wang, G.; Shen, Y.; Cai, H.; Taniguchi, T.; Watanabe, K.; Carrere, H.; Lagarde, D.; et al. Excitonic Linewidth Approaching the Homogeneous Limit in MoS_2-Based van Der Waals Heterostructures. *Phys. Rev. X* **2017**, *7* (2), 021026.
(35) Hoshi, Y.; Kuroda, T.; Okada, M.; Moriya, R.; Masubuchi, S.; Watanabe, K.; Taniguchi, T.; Kitaura, R.; Machida, T. Suppression of Exciton-Exciton Annihilation in Tungsten Disulfide Monolayers Encapsulated by Hexagonal Boron Nitrides. *Phys. Rev. B: Condens. Matter Mater. Phys.* **2017**, *95* (24), 2414013.
(36) Alharbi, A.; Zahl, P.; Shahrjerdi, D. Material and Device Properties of Superacid-Treated Monolayer Molybdenum Disulfide. *Appl. Phys. Lett.* **2017**, *110* (3), 033503.
(37) Lien, D. H.; Uddin, S. Z.; Yeh, M.; Amani, M.; Kim, H.; Ager, J. W.; Yablonovitch, E.; Javey, A. Electrical Suppression of All Nonradiative Recombination Pathways in Monolayer Semiconductors. *Science* **2019**, *364* (6439), 468−471.
(38) Schaibley, J. R.; Yu, H.; Clark, G.; Rivera, P.; Ross, J. S.; Seyler, K. L.; Yao, W.; Xu, X. Valleytronics in 2D Materials. *Nat. Rev. Mater.* **2016**, *1* (11), 16055.
(39) Liu, Z.; Amani, M.; Najmaei, S.; Xu, Q.; Zou, X.; Zhou, W.; Yu, T.; Qiu, C.; Birdwell, A. G.; Crowne, F. J.; et al. Strain and Structure Heterogeneity in MoS_2 Atomic Layers Grown by Chemical Vapour Deposition. *Nat. Commun.* **2014**, *5*, 5246.
(40) Wei, K.; Liu, Y.; Yang, H.; Cheng, X.; Jiang, T. Large Range Modification of Exciton Species in Monolayer WS_2. *Appl. Opt.* **2016**, *55* (23), 6251.
(41) Mitioglu, A. A.; Plochocka, P.; Jadczak, J. N.; Escoffier, W.; Rikken, G. L. J. A.; Kulyuk, L.; Maude, D. K. Optical Manipulation of the Exciton Charge State in Single-Layer Tungsten Disulfide. *Phys. Rev. B: Condens. Matter Mater. Phys.* **2013**, *88* (24), 245403.
(42) Carozo, V.; Wang, Y.; Fujisawa, K.; Carvalho, B. R.; McCreary, A.; Feng, S.; Lin, Z.; Zhou, C.; Perea-López, N.; Elías, A. L.; et al. Optical Identification of Sulfur Vacancies: Bound Excitons at the Edges of Monolayer Tungsten Disulfide. *Sci. Adv.* **2017**, *3* (4), No. e1602813.
(43) Refaely-Abramson, S.; Qiu, D. Y.; Louie, S. G.; Neaton, J. B. Defect-Induced Modification of Low-Lying Excitons and Valley Selectivity in Monolayer Transition Metal Dichalcogenides. *Phys. Rev. Lett.* **2018**, *121* (16), 1−6.
(44) Addou, R.; McDonnell, S.; Barrera, D.; Guo, Z.; Azcatl, A.; Wang, J.; Zhu, H.; Hinkle, C. L.; Quevedo-Lopez, M.; Alshareef, H. N.; et al. Impurities and Electronic Property Variations of Natural MoS_2 Crystal Surfaces. *ACS Nano* **2015**, *9* (9), 9124−9133.
(45) Atallah, T. L.; Wang, J.; Bosch, M.; Seo, D.; Burke, R. A.; Moneer, O.; Zhu, J.; Theibault, M.; Brus, L. E.; Hone, J.; et al. Electrostatic Screening of Charged Defects in Monolayer MoS_2. *J. Phys. Chem. Lett.* **2017**, *8* (10), 2148−2152.
(46) Cao, Y.; Stavrinadis, A.; Lasanta, T.; So, D.; Konstantatos, G. The Role of Surface Passivation for Efficient and Photostable PbS Quantum Dot Solar Cells. *Nat. Energy* **2016**, *1* (4), 16035.
(47) Zherebetskyy, D.; Scheele, M.; Zhang, Y.; Bronstein, N.; Thompson, C.; Britt, D.; Salmeron, M.; Alivisatos, P.; Wang, L. W. Hydroxylation of the Surface of PbS Nanocrystals Passivated with Oleic Acid. *Science* **2014**, *344* (6190), 1380−1384.
(48) Grandhi, G. K.; Arunkumar, M.; Viswanatha, R. Understanding the Role of Surface Capping Ligands in Passivating the Quantum Dots Using Copper Dopants as Internal Sensor. *J. Phys. Chem. C* **2016**, *120* (35), 19785−19795.
(49) Wang, Y.; Kim, J. C.; Wu, R. J.; Martinez, J.; Song, X.; Yang, J.; Zhao, F.; Mkhoyan, A.; Jeong, H. Y.; Chhowalla, M. Van Der Waals Contacts between Three-Dimensional Metals and Two-Dimensional Semiconductors. *Nature* **2019**, *568* (7750), 70−74.
(50) Desai, S. B.; Madhvapathy, S. R.; Amani, M.; Kiriya, D.; Hettick, M.; Tosun, M.; Zhou, Y.; Dubey, M.; Ager, J. W.; Chrzan, D.; et al. Gold-Mediated Exfoliation of Ultralarge Optoelectronically-Perfect Monolayers. *Adv. Mater.* **2016**, *28* (21), 4053−4058.
(51) Li, H.; Wu, J.; Huang, X.; Lu, G.; Yang, J.; Lu, X.; Xiong, Q.; Zhang, H. Rapid and Reliable Thickness Identification of Two-Dimensional Nanosheets Using Optical Microscopy. *ACS Nano* **2013**, *7* (11), 10344−10353.
(52) Enderlein, J.; Erdmann, R. Fast Fitting of Multi-Exponential Decay Curves. *Opt. Commun.* **1997**, *134* (1−6), 371−378.
(53) Momma, K.; Izumi, F. VESTA 3 for Three-Dimensional Visualization of Crystal, Volumetric and Morphology Data. *J. Appl. Crystallogr.* **2011**, *44*, 1272.

DOI: 10.1021/acs.nanolett.9b02431
Nano Lett. 2019, 19, 6299−6307